T.A. Porter, G. P. Rowell, G. Jóhannesson, and I.V. Moskalenko
Galactic PeVatrons and helping to find them: effects of galactic absorption on the observed spectra of very high energy γ -ray sources
Physical Review D, 2018; 98(4):1-6

Originally published by American Physical Society at:
http://dx.doi.org/10.1103/PhysRevD.98.041302

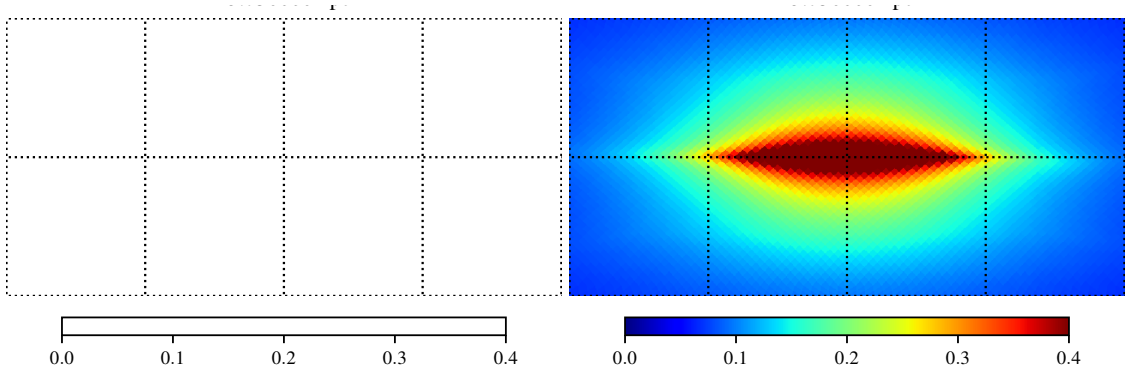

FIG. 1: Optical depth (Eq. 1) at 100 TeV for the R12 (left) and F98 (right) ISRF models for an integration path length of 23.5 kpc. The maps are in cartesian projection covering Galactic coordinates $90^\circ \quad l \quad 90^\circ$ and $45^\circ \quad b \quad 45^\circ$ with $l, b = 0^\circ, 0^\circ$ at the centre. The longitude meridians and latitude parallels have 45° spacing. Note that the scale saturates at an optical depth of 0.4 for ease of visual comparison between the R12 and F98 predictions (the F98 model produces optical depths higher than 0.4 for this distance horizon toward the inner Galaxy).

viding a reasonable agreement with the data from near to far-infrared wavelengths. So, at the present stage of modelling, the R12 and F98 models can be considered to provide reasonable bounds on the intensity distributions of low-energy photons in the Galaxy. For VHE γ-ray sources located toward, or beyond, the inner Galaxy the variance in the predicted infrared photon distributions will produce correspondingly different pair-absorption effects motivating the consideration of both models in this paper.

The spectral intensity for either ISRF model at each point in space is represented using a HEALPix Nside = 8 map with 256 logarithmic wavelength grid points per pixel from 0.1 to 10000 μm. The spatial sampling is over a Galactocentric cylindrical grid with spacing that is variable in R and Z, and remains constant azimuthally. (There are 44 radial bins sampling 0 to 30 kpc, 1 Z-bin for the plane and 8 additional above/below sampling to $\pm$20 kpc, and 36 azimuthal bins.) Evaluation of the spectral intensity at all points x in Eq. (1) for this component is made for either model using tri-linear interpolation. The CMB is modelled as a spatially constant blackbody with temperature $T_{\rm CMB} = 2.725$ K.

Figure 1 shows the optical depth for the ISRF models at a γ-ray energy of 100 TeV for an integration path length of 23.5 kpc, the far side of the Galaxy stellar disc. This is within the expected distance that the forthcoming CTA facility is expected to be able to discriminate spectral features $\gtrsim$ 10 TeV [19]. For this distance the optical depth is non-negligible for Galactic longitudes $-90^\circ \lesssim l \lesssim 90^\circ$ and latitudes $-45^\circ \lesssim b \lesssim 45^\circ$, and its distribution on the sky reflects that of the infrared photons predicted by the two ISRF models inside the Solar circle. The optical depth is highest for the R12 model for longitudes $l \sim \pm 30^\circ$, which are lines of sight intersecting where the starlight from the spiral arms combines with the peak of the dust density distribution to produce the maximum of infrared emissions around $R \sim 4$ kpc, as discussed above. Similarly, the higher infrared emissions for the F98 model over the inner Galaxy produce the correspondingly larger optical depths that peak toward the GC. For both ISRF models there is a small amount of asymmetry in the optical depth maps about the $l = 0^\circ$ meridian caused by the spiral arms (R12) or stellar bar (F98) – see Fig. 7 from Porter et al. [15] for the spatial distribution of their integrated energy densities at the Galactic plane, which illustrates the asymmetrical features for the two ISRF models.

Figure 2 shows the transmittance ($\exp[-\tau_{\gamma\gamma}(E)]$) for both ISRF models toward the GC at two distances folded with a sub-exponential cutoff function $\propto \exp(-[E/E_{\rm cut}]^{0.5})$ following Kelner et al. [20] with $E_{\rm cut} = 100$, 316, 562 TeV, and the no-cutoff case, respectively. Here the underlying CR proton power-law spectrum has an exponential term $\propto \exp(-E/E_{\rm cut,p})$ with cutoff energy $E_{\rm cut,p}$ that is approximately an order of magnitude higher than $E_{\rm cut}$. The unattenuated curves are shown as solid lines, with the broken lines showing the effect of ISRF-only (short-dashed) and combined ISRF/CMB (long-dashed) attenuation. For a source located at the GC (using the IAU-recommended Sun-GC distance of 8.5 kpc [21]) the F98 model produces about twice the attenuation compared to the R12 model around 100 TeV (transmittance $\sim$ 0.85/0.7 for R12/F98).

The attenuation curves without cutoff illustrate the range of the likely effect for the ISRF models at different distances. For a source located at the GC the pair-absorption effect mimics to some degree a spectrum with an intrinsic cutoff. Only using information from the $10 - 100$ TeV energy range the γ-ray "cutoff" energy is $\sim$ 500/1000 TeV (F98/R12). For the case where the spectrum at source does have a cutoff the pair absorption

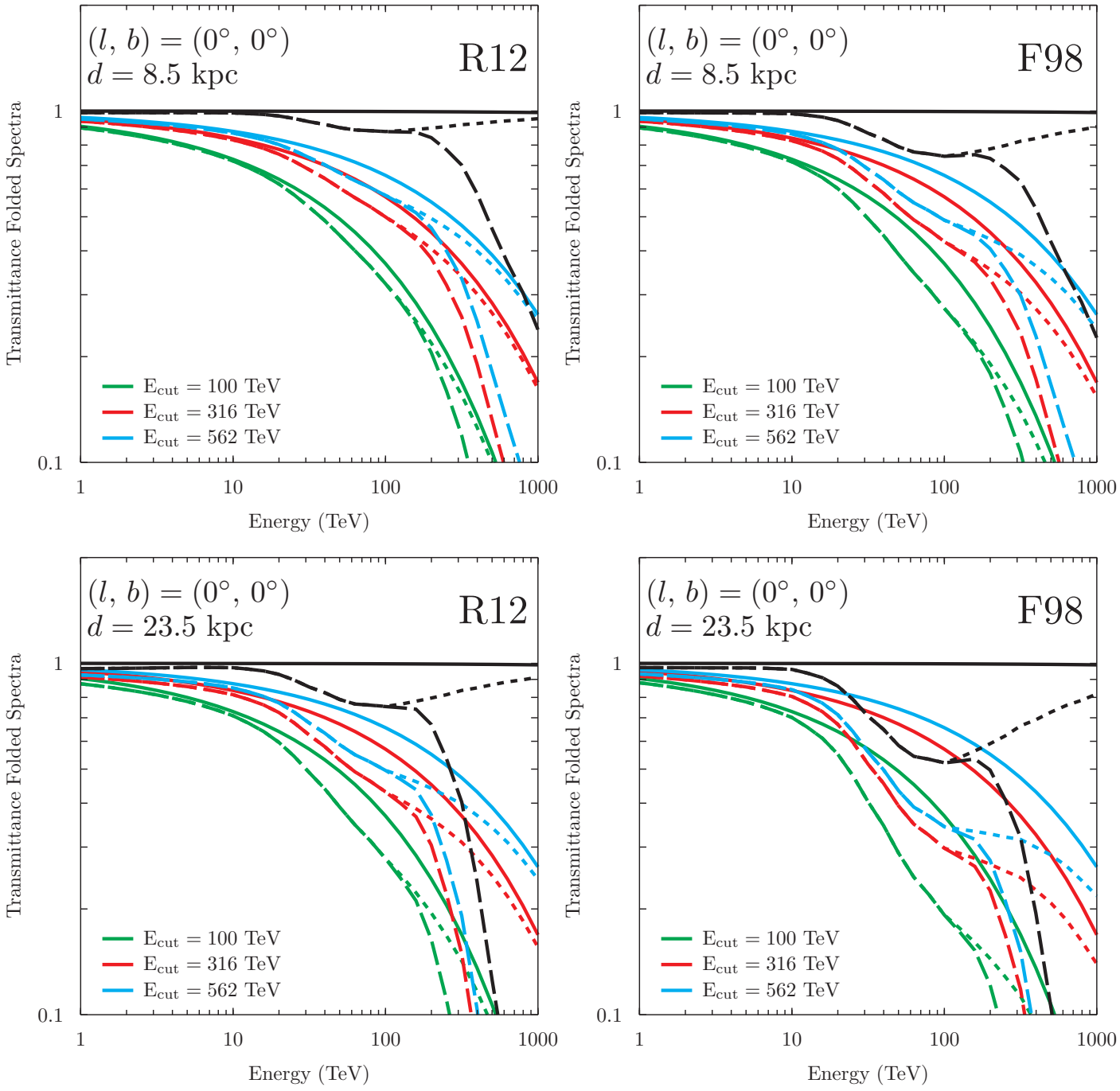

FIG. 2: Transmittance folded spectra for the R12 (left) and F98 (right) ISRF models for a source located at a distance 8.5 kpc (top) and 23.5 kpc (bottom) for the direction $(l, b) = (0°, 0°)$ in Galactic coordinates for selected exponential cutoff energies. Line styles: solid, no attenuation; short-dashed, ISRF-only attenuation; long-dashed, ISRF+CMB attenuation. Colours other than black are for cutoff energies $E_{\rm cut}$: green, 100 TeV; cyan, 316 TeV; red, 562 TeV. Note that the solid curves for all panels are identical.

steepens the spectrum further so that its observed shape appears as if the intrinsic cutoff has a lower γ-ray energy. For a source located at the GC the downward shift for the inferred cutoff energy is between a factor ~ 2 (e.g., cyan and red long-dashed curves for R12) and ~ 5 (e.g., cyan and red long-dashed curves for F98). For more distant sources the steepening can be more severe (see lower panels of Fig. 2). Because γ-ray data has finite energy resolution extracting unique cutoff energies is non-trivial due to the different low-energy photon distribution for the ISRF models.

Discussion: Correction for the pair absorption always

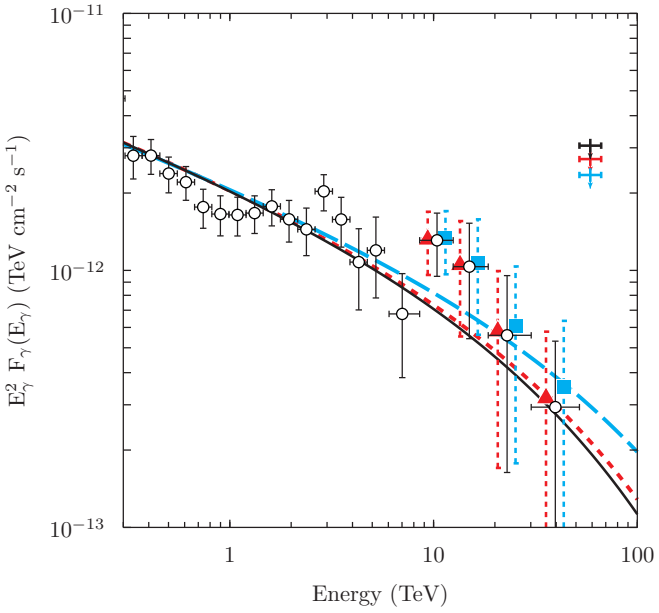

FIG. 3: Spectrum of the "diffuse" emissions toward the GC measured by the HESS instrument [6] together with absorption-corrected data (note only absorption-corrected points > 10 TeV are shown and these are offset compared to the original data by -10% (R12) and +10% (F98) in energy, respectively, for clarity). Point styles and colours: black open, uncorrected; red solid triangle, R12; cyan solid square, F98. Lines show the γ-ray spectral fit models used to estimate the 95% lower confidence level to the proton cutoff energies (see text). Line types: solid, no ISRF correction; short-dashed, R12; long-dashed, F98.

produces harder instrinsic spectra $\gtrsim$ 10 TeV than observed. Accounting for this effect can therefore affect the interpretation for the origin of γ-ray emissions from a source. To see this the HESS data toward the GC for the "diffuse" spectrum attributed to the PeVatron there are ISRF-corrected and refit to obtain revised intrinsic spectral cutoff energy estimates. Figure 3 shows the measured and ISRF-corrected data (note that the ISRF-corrected data are offset in energy by -10% (R12) and +10% (F98), respectively). The `naima` package [22] is used to derive the one-sided 68% and 95% lower confidence bands assuming a sub-exponential cutoff function for the γ-ray spectrum (the fitted power-law index for all three cases is found to be Γ=2.3)[1]. Then, based on the procedure from Abramowski et al. [6], `naima` is also used to provide the underlying CR proton spectral cutoff energy for a γ-ray spectral model with $\Gamma = 2.3$ and lowest cutoff energy fitting within each confidence band. Figure 3 shows the γ-ray spectral models conforming to the 95% confidence lowest cutoffs derived from the original and absorption-corrected data. The resulting lower limits to the CR proton cutoff energies $E_{\rm cut,p}$ (TeV) are found to be (68%/95% = 2680/590; 3870/670; 5550/1180) for the no-ISRF, R12, and F98 cases, respectively. The results obtained for the fits without ISRF model correction are consistent with the published values by Abramowski et al. [6] within the ∼15 to 20% systematic error found from altering the `naima` fit contraints and the method used to find the model function within each confidence band. Thus it is found in this paper that the corrected $E_{\rm cut,p}$ limits are shifted higher by factors ∼1.3 to 2.1 (R12/F98), and the 95% confidence lower limit for $E_{\rm cut,p}$ reaches beyond 1 PeV for the F98 case. Therefore, even though the pair-absorption correction provides only a modest upshift for the fluxes at the highest γ-ray energies measured for this source, the impact on the derived cutoff limit is non-negligible. If the CRs are linked to the central supermassive black hole, the increased CR proton cutoff energy will have follow-on implications for the parameters of the accelerator (e.g., magnetic field, black hole mass and/or acceleration region distance from the black hole – see Aharonian and Neronov [23]). Such implications will become more apparent as future γ-ray observations probe deeply beyond 100 TeV energies. Note that the hardening of the intrinsic spectrum $\gtrsim$ 10 TeV following the pair-absorption correction strengthens the case against a leptonic origin for the emissions, because the rapid cooling on the intense radiation and magnetic fields about the GC region produce softer spectra for this scenario.

Comparing the pair-absorption calculations with other recent works, the transmittance for a source located at the GC for the F98 model is comparable to that obtained by Popescu et al. [14] (their Fig. 15, left panel), while the R12 model is slightly lower than obtained by Vernetto and Lipari [13] (their Fig. 12). It should be emphasised, though, that R12 and F98 are equivalent solutions for the Galaxy-wide ISRF using fully 3D calculations with the same radiation transfer code but different stellar/dust density distribution, while achieving similar agreement with the near- to far-infrared observations. As discussed earlier the models cannot be arbitrarily modified to produce much lower or higher infrared photon densities, particularly over the inner Galaxy, and the calculations made in this paper can therefore be considered to provide likely bounds on the pair attenuation relevant for TeV γ-ray measurements.

The forthcoming CTA TeV γ-ray facility is expected to detect and measure spectra from sources right across the Galaxy (see Sec. 10.4 of [19]). Even for the ISRF model with the lowest absorption (R12) the correction

[1] The reduced χ^2/dof ∼ 1 for a pure power-law fit. When a power-law + sub-exponential cutoff function is fitted a similar χ^2/dof is also obtained, but with a cutoff beyond 1000 PeV (limited by the imposed cutoff parameter upper bound), hence the motivation to provide a confidence band on the cutoff lower limit as per the method outlined by Abramowski et al. [6]. The quality of the spectral fits is not lowered when the pair-absorption correction is applied.

will be important for assessing intrinsic spectral characteristics with γ-ray data up to ~ 200 TeV, below the energies where CMB attenuation is important, but where the ISRF attenuation factor can reach $\sim 50\%$ for a source on the other side of the Galaxy. For the currently operating HAWC instrument with improvements in its spectral reconstruction $\gtrsim 10$ TeV [24] the pair-absorption corrections may also be similarly important, given the expectation to detect sources beyond 100 TeV energies. To aid assessments of the effect on VHE γ-ray spectra the full set of all-sky optical depth maps in energy and distance for the R12 and F98 models calculated in this paper will be available from the GALPROP website, https://galprop.stanford.edu.

Putting these points together, $\gtrsim 10$ TeV γ-ray observations with future instruments of a population (100s as could be expected) of sources across the Galaxy will also reveal the 3D structure of the ISRF. Such observations can be used for optimising the description of the low-energy photon distribution in the Galaxy, providing complementarity to other studies that more commonly employ near- to far-infrared data.

Acknowledgements: TAP and IM acknowledge partial support via NASA grant NNX17AB48G.

The `naima` package is available at http://naima.readthedocs.io/en/latest/radiative.html.

Some of the results in this paper have been derived using the HEALPix [25] package.

[1] V. L. Ginzburg and S. I. Syrovatskii, The Origin of Cosmic Rays (1964).

[2] V. S. Berezinskii, S. V. Bulanov, V. A. Dogiel, and V. S. Ptuskin, Astrophysics of cosmic rays (1990).

[3] A. R. Bell and S. G. Lucek, MNRAS **321**, 433 (2001).

[4] A. R. Bell, K. M. Schure, B. Reville, and G. Giacinti, MNRAS **431**, 415 (2013), 1301.7264.

[5] S. Thoudam, J. P. Rachen, A. van Vliet, A. Achterberg, S. Buitink, H. Falcke, and J. R. Hörandel, A&A **595**, A33 (2016), 1605.03111.

[6] A. Abramowski, F. Aharonian, F. A. Benkhali, A. G. Akhperjanian, E. O. Angüner, M. Backes, A. Balzer, Y. Becherini, J. B. Tjus, and et al., Nature (London) **531**, 476 (2016), 1603.07730.

[7] F. Aharonian, R. Yang, and E. de Oña Wilhelmi, ArXiv e-prints (2018), 1804.02331.

[8] Y.-Q. Guo, Z. Tian, Z. Wang, H.-J. Li, and T.-L. Chen, Astrophys. J. **836**, 233 (2017), 1604.08301.

[9] R. J. Protheroe, MNRAS **221**, 769 (1986).

[10] I. V. Moskalenko, T. A. Porter, and A. W. Strong, ApJL **640**, L155 (2006), astro-ph/0511149.

[11] J.-L. Zhang, X.-J. Bi, and H.-B. Hu, A&A **449**, 641 (2006), astro-ph/0508236.

[12] T. A. Porter and A. W. Strong, International Cosmic Ray Conference **4**, 77 (2005), astro-ph/0507119.

[13] S. Vernetto and P. Lipari, Phys. Rev. D **94**, 063009 (2016), 1608.01587.

[14] C. C. Popescu, R. Yang, R. J. Tuffs, G. Natale, M. Rushton, and F. Aharonian, MNRAS **470**, 2539 (2017), 1705.06652.

[15] T. A. Porter, G. Jóhannesson, and I. V. Moskalenko, Astrophys. J. **846**, 67 (2017), 1708.00816.

[16] J. M. Jauch and F. Rohrlich, The theory of photons and electrons. The relativistic quantum field t (1976).

[17] T. P. Robitaille, E. Churchwell, R. A. Benjamin, B. A. Whitney, K. Wood, B. L. Babler, and M. R. Meade, A&A **545**, A39 (2012), 1208.4606.

[18] H. T. Freudenreich, Astrophys. J. **492**, 495 (1998), astro-ph/9707340.

[19] Cherenkov Telescope Array Consortium, ArXiv e-prints (2017), 1709.07997.

[20] S. R. Kelner, F. A. Aharonian, and V. V. Bugayov, Phys. Rev. D **74**, 034018 (2006), astro-ph/0606058.

[21] F. J. Kerr and D. Lynden-Bell, MNRAS **221**, 1023 (1986).

[22] V. Zabalza, Proc. of International Cosmic Ray Conference 2015 p. 922 (2015), 1509.03319.

[23] F. Aharonian and A. Neronov, Astrophys. J. **619**, 306 (2005), astro-ph/0408303.

[24] S. Stephens Marinelli and J. Goodman, ArXiv e-prints (2017), 1708.03502.

[25] K. M. Górski, E. Hivon, A. J. Banday, B. D. Wandelt, F. K. Hansen, M. Reinecke, and M. Bartelmann, Astrophys. J. **622**, 759 (2005), astro-ph/0409513.